JOURNAL OF GEOPHYSICAL RESEARCH, VOL. 114, A05308, doi:10.1029/2009JA014060, 2009

Intra-annual variation of wave number 4 structure of vertical E × B drifts in the equatorial ionosphere seen from ROCSAT-1

Zhipeng Ren,[1,2,3] Weixing Wan,[1] Libo Liu,[1] and Jiangang Xiong[1]

Received 9 January 2009; revised 21 March 2009; accepted 16 April 2009; published 23 May 2009.

[1] This paper studies the intra-annual variation of the wave number 4 structure in the equatorial vertical **E** × **B** drifts at high solar flux level based on of the ROCSAT-1 observations during the interval from 1999 to 2004. It is found that the daytime longitudinal structure is significant in northern summer and early autumn but weak in northern winter. This is consistent with the intra-annual variations of the tidal mode DE3. At night, the intra-annual variation of the wave number 4 structure shows some differences from that in daytime, which may relate to different dynamo mechanisms operating in different local time. We also found that the wave number 4 structure mainly shifts eastward during daytime in most of months, which is coincident with the eastward propagation of the DE3 tide. However, it is largely disturbed near sunrise and sunset. We attribute this disturbance as the jumping of the main dynamo region between *E* and *F* layers, as well as the different dynamo mechanisms in different dynamo regions.

Citation: Ren, Z., W. Wan, L. Liu, and J. Xiong (2009), Intra-annual variation of wave number 4 structure of vertical **E** × **B** drifts in the equatorial ionosphere seen from ROCSAT-1, *J. Geophys. Res.*, *114*, A05308, doi:10.1029/2009JA014060.

1. Introduction

[2] The low-latitude ionosphere is a highly dynamical environment that exhibits significant variations with altitude, latitude, longitude, local time, season, solar cycle, and geomagnetic activity. The coupling processes between the ionosphere and the atmosphere below play important roles in these variations. Recently, using the nightglow images of OI 135.6 nm, *Sagawa et al.* [2005] and *Henderson et al.* [2005] individually observed the wave number 4 longitudinal structure in the equatorial ionization anomaly (EIA). These wave number 4 patterns were also been noticed in total electron content (TEC) and electron density in the low-latitude ionosphere [e.g., *Lin et al.*, 2007a, 2007b; *Liu and Watanabe*, 2008; *Kil et al.*, 2008; *Pedatella et al.*, 2008; *Ren et al.*, 2008; *Scherliess et al.*, 2008; *Wan et al.*, 2008; *Liu et al.*, 2009]. A number of researchers had studied the intra-annual variability of these wave number 4 patterns [e.g., *Kil et al.*, 2008; *Pedatella et al.*, 2008; *Ren et al.*, 2008; *Scherliess et al.*, 2008; *Wan et al.*, 2008; *Liu et al.*, 2009]. Similar structure even occurred in other ionospheric and thermospheric parameters, such as the equatorial electrojet (EEJ), the vertical **E** × **B** plasma drifts ($V_\perp$), the plasma bubble (PB) occurrence rates, the electron temperature, the vertical scale height (VSH), the nitric oxide density in the low thermosphere and zonal neutral wind in the *F* region [e.g., *England et al.*, 2006b; *Fejer et al.*, 2008; *Hartman and Heelis*, 2007; *Kil et al.*, 2007; *Lühr et al.*, 2007, 2008; *Li et al.*, 2008; *Liu et al.*, 2008; *Oberheide and Forbes*, 2008b; *Ren et al.*, 2008].

[3] The wave number 4 patterns in the low-latitude ionosphere could not be explained by longitudinal variations of the geomagnetic fields, which were previously considered as the main reasons responsible to the longitudinal ionospheric structure. Instead, it was explained in terms of the coupling process between the ionosphere and the atmosphere below. *Sagawa et al.* [2005] postulated that the *E* region nonmigrating semidiurnal tide [*Hagan and Forbes*, 2003] should be the origin of the wave number 4 structure in *F* region. *England et al.* [2006a] further demonstrated a clear correspondence between the nonmigrating diurnal tides [*Hagan and Forbes*, 2002] and the morphology of the post sunset EIA. *Immel et al.* [2006] pointed out that the peak locations of this longitudinal structure are coincident with those of the diurnal tidal amplitude predicted by the Global Scale Wave Model (GSWM) [*Hagan and Forbes*, 2002]. They further proposed this structure as the effects of the eastward propagating zonal wave number 3 diurnal tide (DE3), which can achieve large amplitude in the ionospheric *E* region [*Forbes et al.*, 2008; *Oberheide and Forbes*, 2008a].

[4] DE3 is excited by latent heat release associated with raindrop formation in the tropical troposphere [*Hagan and Forbes*, 2002; *Oberheide and Forbes*, 2008a]. It propagates vertically and is sometimes the single largest tidal component above the mesopause [*Forbes et al.*, 2008; *Oberheide and Forbes*, 2008a]. Because there are growing observational evidences that DE3 is the main source of the wave number 4 structure in the ionosphere, DE3 has attracted a considerable attention. Recently, the satellite observations

[1]Beijing National Observatory of Space Environment, Institute of Geology and Geophysics, Chinese Academy of Sciences, Beijing, China.
[2]Wuhan Institute of Physics and Mathematics, Chinese Academy of Sciences, Wuhan, China.
[3]Graduate School of Chinese Academy of Sciences, Beijing, China.

0148-0227/09/2009JA014060$09.00

reveal the climatology of nonmigrating tides including DE3. *Forbes et al.* [2003a, 2003b] and *Oberheide et al.* [2006] found that the zonal wind of DE3 is stronger and occurs primarily during northern summer and autumn, while the meridional component is relatively weaker and occurs primarily during the northern winter. *Oberheide and Forbes* [2008a, 2008b] found that the seasonal change of the temperature fluctuation of DE3 is very similar to that of the zonal wind component, and pointed out that the intra-annual DE3 variation should be interpreted in terms of latitudinally symmetric versus antisymmetric modes (Hough modes). Recent studies have shown that similar intra-annual variations are observed in the wave number 4 structure in the ionization parameters and the DE3 tide. For example, *Wan et al.* [2008] found that the seasonal variation of the wave number 4 patterns of TEC in the low latitude is consistent with that of the zonal wind of the nonmigrating tide mode DE3. *Kil et al.* [2008] compared the amplitude of the DE3 tide at 110 km altitude with the power of the wave number 4 component in the density structure and found that they show similar intra-annual variations.

[5] *Immel et al.* [2006] first proposed a production mechanism of the ionospheric wave number 4. First, the DE3 tide, when propagates into the ionospheric *E* region, can affect the dynamos and lead to modulations on the ionospheric zonal electric fields and $V_\perp$. Then the modulated plasma drifts further induce the motion and redistribution of the ionospheric plasma in *F* region and finally produce the observed longitudinal structure [see also *Kil et al.*, 2007; *England et al.*, 2008; *Oh et al.*, 2008]. This mechanism has been demonstrated by simulations with the TIME-GCM model [*Hagan et al.*, 2007]. The simulation by *Jin et al.* [2008] further indicates that the wave number 4 structure in zonal electric field is directly from charge separation induced by the Hall current, which is driven by the zonal wind of DE3. At the same time, observations also show that the wave number 4 structures exist indeed in parameters of the ionospheric electric fields (EEJ and $V_\perp$) [e.g., *England et al.*, 2006b, *Hartman and Heelis*, 2007; *Kil et al.*, 2007; *Fejer et al.*, 2008].

[6] At middle and low latitudes, the ionospheric electric fields, hence the $\mathbf{E} \times \mathbf{B}$ drifts, are mainly driven by *E* region dynamos, and sometimes (especially in nighttime) also by *F* region dynamos [e.g., *Heelis*, 2004]. In turn, the *E* region dynamo is driven mainly by the tidal winds that come from below, while the *F* region dynamo is driven mainly by neutral winds driven by the in situ heating. The ionospheric electric fields play an important role in the ionospheric and thermospheric dynamics. In fact, the ionospheric electric fields and the $\mathbf{E} \times \mathbf{B}$ drifts redistribute the plasma density to form the EIA through the fountain effect and affect the thermospheric neutral winds. As the tidal winds that come from below can drive the ionospheric dynamos, the ionospheric dynamo is also an important mechanism in the coupling between the ionosphere and the atmosphere below. As the wave number 4 structures in the ionization parameters depend on that in $V_\perp$ which is correlated with the DE3 tide, the wave number 4 structure in $V_\perp$ may show similar intra-annual variations to the other two phenomena. Here, we will explore the intra-annual variation of the wave number 4 structure in $V_\perp$ using the vertical plasma drifts velocity observed by ROCSAT-1.

2. Measurements and Data Processing

[7] ROCSAT-1 has a circular orbit at an altitude of about 600 km with an inclination of 35°. The period of an orbit is about 97 min, and consecutive orbits are separated in longitude by about 24.5°. The 24-h local times are covered in the latitude $-35°\sim35°$ every 25 days. This satellite carries Ionospheric Plasma and Electrodynamics Instrument (IPEI), which is designed to take in situ measurements of ion density, temperature, composition, and drift velocity, over a large dynamic range with high accuracy, to monitor the behavior of plasma. The cross-track plasma drift velocity is measured with the onboard ion drift meter (IDM). ROCSAT-1 was launched on 27 January 1999, and the equatorial *F* region plasma drifts were continuously measured by IPEI from mid-March 1999 to early June 2004. The accuracy of the cross-track plasma drift velocity measurements from this IDM depends on the total ion density and the proportion of oxygen ions. The cross-track plasma drift velocity can be determined accurately (error <10%) when the total ion density is greater than 10^3 cm^{-3} and the percentage of the oxygen ion exceeded 85%. Because of the near horizontal magnetic field near the dip equator, the equatorial *F* region vertical plasma drifts correspond basically to the electrodynamic drift driven by the zonal ionospheric electric fields. Here, we will use the observations of vertical $\mathbf{E} \times \mathbf{B}$ plasma drifts ($V_\perp$) near the dip equator from 1999 to 2004.

[8] Only measurements of $V_\perp$ within 5° of the dip equator have been used, since they have higher statistical significance. Observations taken during periods of high magnetic activity marked by the $K_p > 3$ were additionally removed from the data set in order to confine our attention to quiet time variations. As *Fejer et al.* [2008] had done, we only using $V_\perp$ corresponding to total ion density larger than 10^5 cm^{-3} between 0800 LT and 0200 LT, and larger than 5×10^4 cm^{-3} from 0200 LT to 0800 LT, which maximized both the accuracy of the measurements during daytime and the number of late night observations. To minimize the effects of equatorial plasma depletions, $V_\perp$ with magnitudes larger than 100 m/s are removed. We first separate $V_\perp$ data into 12 month bins (from January to December) which are all 2 months overlapping 3 months wide bins. Then, we binned them into 20° overlapping 30° wide geographical longitudinal bins. As $V_\perp$ varies with solar flux, to better explore the intra-annual variations, we must remove the effect of solar activity. *Fejer et al.* [2008] developed a quiet time equatorial *F* region vertical plasma drift model based on ROCSAT-1 observations. Here, to remove the effect of solar activity, we first use a similar method to calculate the effect of solar flux on $V_\perp$. We only choose $V_\perp$ corresponding to solar 10.7 cm flux index ($F_{10.7}$) between 140 and 210 which we can assume a linear $V_\perp$ dependence with $F_{10.7}$ [see *Fejer et al.*, 2008]. Then, we binned these data into 15 min overlapping 30 min wide bins in the 1700–2200 LT sector and 30 min overlapping 1-h wide bins in other LT sector and calculated the average $V_\perp$ and average $F_{10.7}$. We discarded points outside two standards deviations in every bin. Figure 1 (top) shows all $V_\perp$ data used in this work.

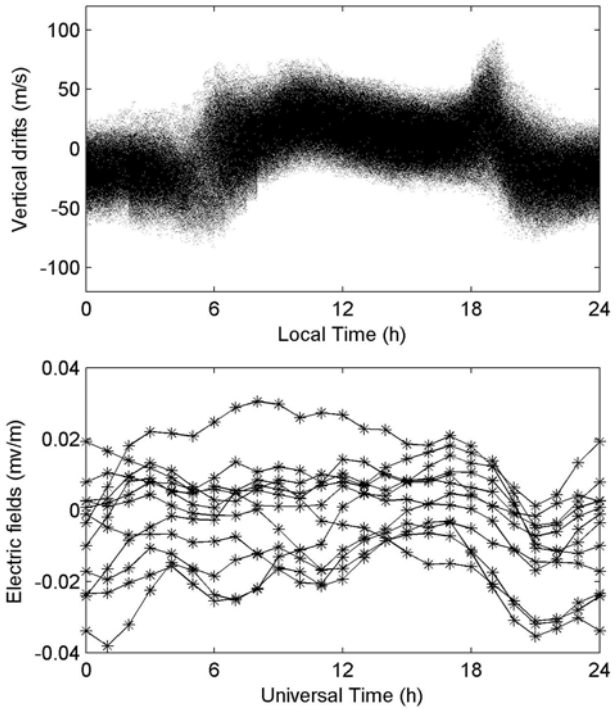

Figure 1. (top) $V_\perp$ pattern observed from ROCSAT-1, which are used in this work. (bottom) Universal time variations of longitudinally average equatorial zonal electric fields in different months.

Then we binned these data into 1-h bins shifted every 30 min in the 1700–2200 LT sector and 4-h local time bins shifted every 1-h in other LT sector once again and calculated the solar flux dependence of $V_\perp$ for every bin. Finally, we performed 3 point running averages on the longitudinal variation of this solar flux dependence. On the basis of these results, we can obtain local time and longitudinal variations of $V_\perp$ for mean solar flux ($F_{10.7}$ = 175) in different months. As zonal electric fields' line integrals along the dip equator must be zero (curl-free condition), we calculate the average zonal electric fields to examine our result. Figure 1 (bottom) shows universal time variations of longitudinally average zonal electric fields in different months. As the equatorial geomagnetic field strength is between 0.19 and 0.30 G at the height of the satellite, the averaged zonal electric fields by about 0.03 mV/m changes the averaged $V_\perp$ by about 1.2 m/s. Since we do not know the exact local time and solar-flux-dependent accuracy of the drift measurements, we did not attempt to correct them to satisfy the curl-free condition.

[9] An example of the above procedure is shown in Figure 2 (top). As show in Figure 2 (top), the longitudinal and local time dependences of $V_\perp$ in October are similar to the equinox result of empirical model developed by *Fejer et al.* [2008]. Since our primary interest is in the wave number 4 longitudinal structure, we use a similar method to *Wan et al.* [2008] to extract this longitudinal component from ROCSAT-1 observation. To obtain the longitudinal wave number spectra, we first perform a spectral analysis on the $V_\perp$. Then, the wave number 4 component is picked out by the inverse Fourier transformation on the obtained spectra in a wave number band from 3.5 to 4.5. Figure 2 (bottom) depicts the Fourier filtered wave number 4 pattern of $V_\perp$ corresponding to the original data shown in Figure 2 (top).

[10] Previous work had suggested that the intra-annual variations of the wave number 4 component in the ionization parameters are consistent with that of DE3 tide [e.g., *Kil et al.*, 2008; *Wan et al.*, 2008]. Thus, we will also investigate the connection of the wave number 4 structure of $V_\perp$ with DE3 tide. As found by *Oberheide and Forbes* [2008a, 2008b], the DE3 tide is strongest in the low-latitude *E* region. Hence, in the following section, we will compare the intra-annual variation of the wave number 4 component of $V_\perp$ with that of the DE3 tides in the TIMED SABER temperature and TIMED TIDI zonal and meridional winds at the height of 100 km. The TIMED SABER instrument is a 10-channel radiometer that retrieves the kinetic temperature from 20 to 120 km altitude on the basis of the CO_2 15.4 μm limb emission measurements [*Russell et al.*, 1999], and the TIMED TIDI instrument is a limb scanner that measures the daytime and nighttime neutral winds in the

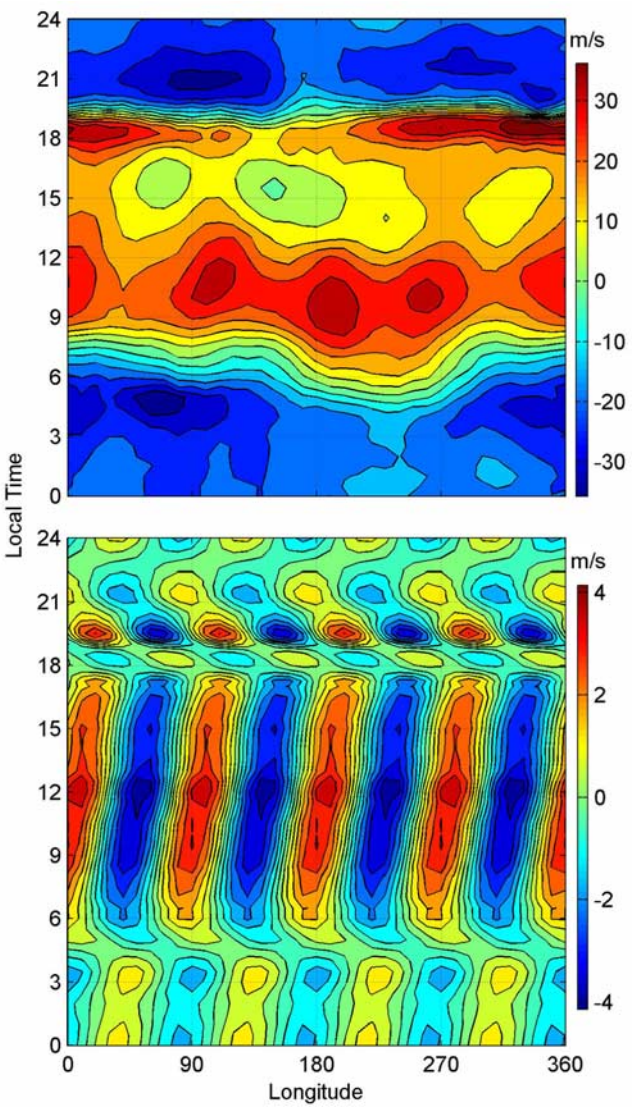

Figure 2. (top) The local time and longitudinal variations of $V_\perp$ in October in units of m/s. (bottom) The Fourier filtered wave number 4 component of $V_\perp$ in October.

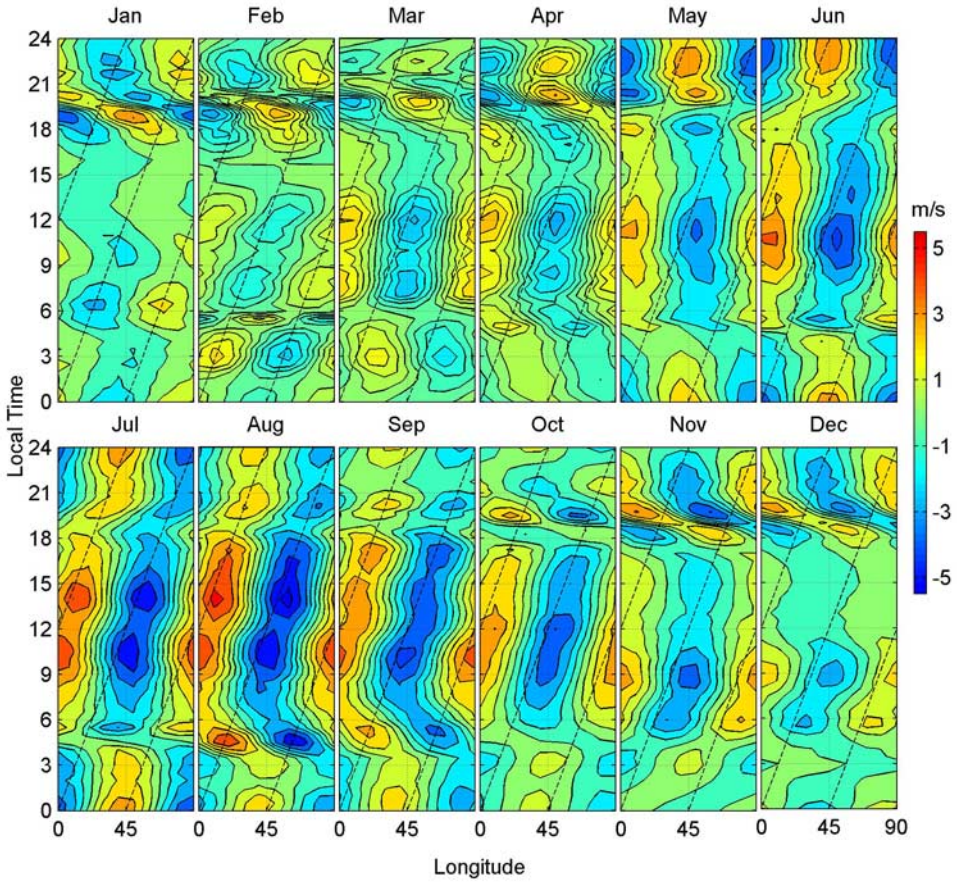

Figure 3. The wave number 4 component filtered from the $V_\perp$ in units of m/s. The columns are for the months of January–December. Because of the recurrence of the wave patterns in the longitude domain, only one-pattern $V_\perp$ maps in a longitude range from 0° to 90° is shown. The slanted dashed lines indicate a longitude of 90° step within 24 h.

MLT region by monitoring the Doppler shift of the various upper atmosphere airglow layers [*Killeen et al.*, 1999]. TIMED SABER and TIMED TIDI observations are both produced by the National Center for Atmospheric Research. The TIMED observations using in this work are from March 2002 to November 2007. TIMED satellite is a slowly processing satellite, and the 24-h local times coverage of the TIMED SABER and TIMED TIDI observations is obtained every 60 days. Hence, the temperature fluctuation, zonal and meridional wind of DE3 tide are first extracted by least squares fitting from a 60 day running window centered on each day. Then, we bin them into 12 1-month wide bins, and the mean amplitudes of DE3 tide in different months can be calculated.

3. Result and Discussions

[11] With the procedures introduced above, we processed the $V_\perp$ data observed by ROCSAT-1, and obtained the Fourier filtered wave number 4 component of the $V_\perp$ at high solar flux level. The local time and longitudinal dependences of the wave number 4 component of $V_\perp$ for different months are displayed in Figure 3. The 12 columns in Figure 3 are for the 12 months from January to December. Because of the recurrence of the wave patterns in the longitude domain (see Figure 2 (bottom)), Figure 3 shows only one-pattern $V_\perp$ maps in longitude range from 0°E to 90°E. The contours in these maps illustrate the absolute values of $V_\perp$ equal to the standard deviation of the wave-field; hence their corresponding locations indicate where the wave patterns are remarkable. As shown in Figure 3, the wave number 4 structure of $V_\perp$ has obviously intra-annual and local time dependences. The intensity of the wave number 4 structure depends very much on season and local time. In most of months, the daytime wave patterns are stronger than those at night. The daytime wave number 4 patterns are very weak in northern winter (December–February). The daytime wave intensity begins to increase in March and becomes stronger in April and May. During northern summer (June–August), the daytime wave patterns are very significant. In northern autumn (September–November), the daytime wave intensity is still strong, but begins to decrease. In summary, the daytime wave intensity is weak in northern winter and strong in northern summer and early autumn; it is increased in northern spring and decreased in later northern autumn. The nighttime wave number 4 structures of $V_\perp$ also appear obviously an intra-annual variation. However, the nighttime wave intensity is strong in northern summer and late spring and weak in other seasons.

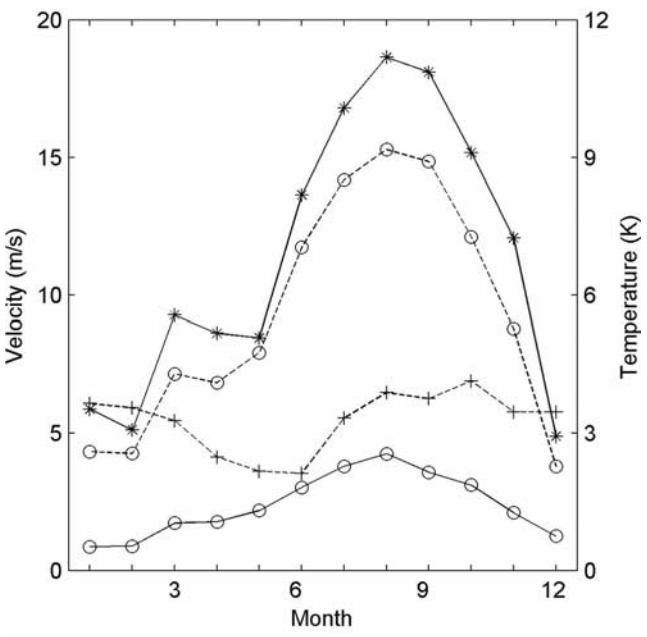

Figure 4. Comparison of the intra-annual variations of the daytime averaged amplitude of the wave number 4 structure of $V_\perp$ (solid line with circles) with the amplitudes of the temperature (dashed line with circles), zonal (solid line with stars), and meridional wind (dashed line with pluses) of DE3 tide at the height of 100 km. $V_\perp$, zonal, and meridional wind are in units of m/s, and temperature is in units of K.

[12] Another important feature in Figure 3 is that the wave number 4 structure mainly shifts eastward as local time increases during daytime in most of months. The slanted dashed lines in Figure 3 indicate a longitude of 90° step within 24 h. By comparing the slope of the wave patterns in Figure 3 with these slanted lines, we will find that the average shifting speed of our wave number 4 structure during daytime (determined by the slope of the wave crests or valleys) in most of months is about 90°/day. However, the daytime wave number 4 structure in northern winter (December–January) don't show obviously eastward shift. We also notice that the wave number 4 structure show obviously phase changes near sunrise and sunset, and the nighttime wave number 4 pattern don't show obviously eastward shift in many months.

[13] The previous works indicate that the wave number 4 structures in the ionization parameters are attributed to the longitudinal modulation of the *F* region vertical plasma drifts [*England et al.*, 2006a, 2008; *Immel et al.*, 2006; *Hagan et al.*, 2007; *Oh et al.*, 2008; *Wan et al.*, 2008]. As the ionization parameters in low latitude are closely associated with the upward $V_\perp$ through the fountain effect, the wave number 4 structures in the ionization parameters mainly vary with the daytime $V_\perp$ which is mainly upward, and the effect of the nighttime $V_\perp$ is weak. Actually, we will find that the intra-annual variations of the wave number 4 patterns of TEC observed by *Wan et al.* [2008] is very similar to that of the daytime wave number 4 structure of $V_\perp$. *Kil et al.* [2008] studied the intra-annual variation of the power of the wave number 4 component in the density structure and found similar intra-annual variations with that of daytime $V_\perp$. The sharp increase of upward $V_\perp$ near 1700–1900 LT, which is known as the prereversal enhancement (PRE), can also affect the fountain effect. However, as shown in our result and suggested by previous works [*Kil et al.*, 2007; *Fejer et al.*, 2008], the wave number 4 structure of $V_\perp$ near PRE is weak. So the intra-annual variations of wave number 4 patterns of TEC mainly vary with that of the daytime $V_\perp$.

[14] The daytime ionospheric electric fields are mainly controlled by *E* region neutral wind dynamos [*Heelis*, 2004]. As suggested by previous works [e.g., *England et al.*, 2006b; *Hagan et al.*, 2007; *Hartman and Heelis.*, 2007; *Kil et al.*, 2007, 2008; *Fejer et al.*, 2008; *Jin et al.*, 2008], it is largely believed that the wave number 4 structure of equatorial daytime $V_\perp$ is the signature of an DE3 tide that is driven by latent heat release in the troposphere [see *Hagan and Forbes*, 2002]. Thus, above intra-annual variation of $V_\perp$ should be also corresponding to the intra-annual variations of DE3 tide in the *E* region. Recently, on the basis of the satellite observations, the climatology of nonmigrating tides including DE3 has been studied. With the HRDI and WINDII instruments on UARS, *Forbes et al.* [2003a, 2003b] found that the zonal wind of DE3 is stronger and occurs primarily during northern summer and autumn, while the meridional component is relatively weaker and occurs during the northern winter. Similar results are also obtained from the analysis of the TIDI data onboard of the TIMED satellite [*Oberheide et al.*, 2006]. In addition, the observation from the TIMED SABER indicates that the seasonal change of the temperature fluctuation of DE3 is very similar to that of the zonal wind component [*Oberheide and Forbes*, 2008a, 2008b]. Similar intra-annual variations in the wave number 4 structure in the ionization parameters and the DE3 tide are observed in a number of researchers. For example, *Wan et al.* [2008] found that the seasonal variation of the wave number 4 patterns of TEC in the low-latitude ionosphere is consistent with that of the zonal wind of the nonmigrating tide mode DE3. *Kil et al.* [2008] compared the amplitude of the DE3 temperature tide at 110 km altitude with the power of the wave number 4 component in the density structure and found that they show similar intra-annual variations. As the wave number 4 component in the density structure depends on the wave number 4 component of $V_\perp$, this result imply that the intra-annual variation of the wave number 4 component of $V_\perp$ relate to the intra-annual variations of the DE3 tide. We also investigate the connection of the wave number 4 component of $V_\perp$ with DE3 tide by comparing the intra-annual variation of their daytime averaged amplitudes with that of the amplitudes of DE3 tide in the TIMED SABER temperature and TIMED TIDI zonal and meridional wind. In Figure 4, we compare the intra-annual variation of the daytime (0700–1700LT) averaged amplitude of the wave number 4 structure of $V_\perp$ (solid line with circles) with the low-latitude averaged (between ±20°geographical latitude) amplitudes of the temperature (dashed line with circles), zonal (solid line with stars) and meridional wind (dashed line with pluses) of DE3 tide at the height of 100 km. As shown in Figure 4, the intra-annual variation of the daytime averaged amplitude of the wave number 4 component of $V_\perp$ is consistent completely with that of the zonal wind and

temperature fluctuations of DE3 at the height of 100 km, and has very little connection with that of the meridional wind component.

[15] As pointed out by *Oberheide and Forbes* [2008a, 2008b], the discrepancy in the seasonal variation between the DE3 components should be interpreted in terms of latitudinally symmetric versus antisymmetric modes (Hough modes). That is, the first symmetric mode, which occurs mainly in northern summer and autumn and can cause a latitudinally symmetric wind pattern, dominate the zonal wind component and the temperature fluctuation, and the first antisymmetric mode, which occurs mainly in northern winter and can cause a latitudinally antisymmetric wind pattern, dominate the meridional wind component. The ionospheric electric fields couple between northern and southern hemispheres along the highly conducting magnetic field lines. Through this coupling, a symmetric wind pattern will drive a symmetric dynamo electric fields ($\mathbf{U} \times \mathbf{B}$, where $\mathbf{U}$ is neutral wind) and produce stronger polarization electric fields, and an antisymmetric wind pattern will drive an antisymmetric dynamo electric fields and produce a weaker polarization electric fields [e.g., *Richmond and Roble*, 1987]. Hence, the wave number 4 structure of $V_\perp$ in northern summer and autumn, when the DE3 wind is mainly a symmetric wind, is stronger than that in northern winter, when the DE3 wind is mainly an antisymmetric wind. Actually, the intra-annual variation of the daytime wave number 4 structure of $V_\perp$ is similar to that of the symmetric modes of the DE3 tide [see *Oberheide and Forbes*, 2008a, 2008b]. So the intra-annual variation of the daytime wave number 4 structure of $V_\perp$ must be corresponding to that of the DE3 tide.

[16] However, the dynamo mechanisms operating during daytime and at night are different. The daytime ionospheric electric fields, hence the daytime $\mathbf{E} \times \mathbf{B}$ drifts, are mainly driven by *E* region dynamo, and the *F* region dynamo plays an important role at night [e.g., *Heelis*, 2004]. In turn, the *E* region dynamo is driven mainly by the tidal winds that come from below, while the *F* region dynamo is mainly by neutral winds driven by the in situ heating. The generation mechanism for the wave number 4 structure of $V_\perp$ in different local time should also be different. By using a numerical model of atmospheric electrodynamics with input fields from a whole atmosphere general circulation model and an ionosphere-thermosphere model, *Jin et al.* [2008] studied the generation mechanism for the wave number 4 structure of the *F* region zonal electric field with respect to the DE3 tide that originates from the convective activities in the troposphere and propagates upward. They found that the daytime wave number 4 structure of zonal electric field is a direct result from charge separation induced by the Hall dynamo current driven by the zonal DE3 wind around the height of peak Hall conductivity, and those during at nigh are rather produced to satisfy the electrostatic condition driven by the zonal DE3 wind in the *F* region during the nighttime. So the intra-annual variation of the nighttime wave number 4 structures shows some differences from those during daytime.

[17] As shown in Figure 3, in most of months, the daytime wave number 4 structure of $V_\perp$ mainly shifts eastward with an average shifting speed of nearly 90°/day. *Wan et al.* [2008] found that the wave number 4 patterns of TEC in the low-latitude latitude also shift eastward with an average shifting speed of nearly 90°/day. They suggested that this eastward shift of the wave number 4 patterns of TEC is related to the eastward propagation of the causative nonmigrating tides (DE3) in the *E* region. The related shifting speed (phase speed) of DE3 is 120°/day in UT frame, or 90°/day in LT frame [*Hagan and Forbes*, 2002; *Forbes et al.*, 2008]. If we consider DE3 as the primary source of our wave number 4 structure of $V_\perp$, the related shifting speed should also be 90°/day, which is approximately the average shifting speed of our wave number 4 structure in our observations. However, the dynamo mechanisms operating during daytime and at night are different, and the main dynamo region jumps between *E* and *F* layers near sunrise and sunset. As the nighttime wave number 4 patterns of $V_\perp$ are mainly driven by the *F* region dynamo [*Jin et al.*, 2008], the nighttime wave number 4 structure of $V_\perp$ doesn't show obviously eastward shift in many months. The obvious phase changes of the wave number 4 structure of $V_\perp$ near sunrise and sunset may also relate to the different dynamo mechanisms operating in different periods of local time. The largely phase disturbance near sunrise and sunset is attributed to the jumping of the main dynamo region between *E* and *F* layers, as well as the different dynamo mechanism in different dynamo regions. Similar eastward shift and the sudden phase changes near sunrise and near sunset also have been found by *Jin et al.* [2008] in their simulation results. They also suggested that the eastward shift relates to the eastward propagation of the DE3, and the sudden phase changes are caused by the transition of dynamo region and mechanism. So the eastward shift of the daytime wave number 4 structure is caused by the eastward propagation of the DE3 and the phase largely disturbance near sunrise and sunset is attributed to the transition of dynamo region and mechanism.

4. Summary and Conclusion

[18] In the present work, the vertical plasma drifts velocities observed by ROCSAT-1 from 1999 to 2004 are used to study the intra-annual variation of the wave number 4 structure of equatorial vertical $\mathbf{E} \times \mathbf{B}$ plasma drifts ($V_\perp$) at high solar flux level. We first obtained local time and longitudinal variations of $V_\perp$ for high solar flux ($F_{10.7} = 175$) in different months and then Fourier filtered to obtain the wave number 4 component. Through studying in detail the diurnal and intra-annual variations of the wave patterns, we found that the daytime longitudinal structure is significant in northern summer and early autumn, but weak in northern winter. This intra-annual variation is consistent with those of the tidal mode DE3. The intra-annual variation of the nighttime wave number 4 structures show some differences from those during daytime, which relate to the different dynamo mechanisms operating during different period of local time. We also found that the wave number 4 structure mainly shifts eastward during daytime in most of months, which is caused by the eastward propagation of the DE3 tide; the phase largely disturbed near sunrise and sunset, which is attributed to the jumping of the main dynamo region between *E* and *F* layers, as well as the different dynamo mechanism in different dynamo regions. In conclusion, the intra-annual variation of the wave number 4

structure of $V_\perp$ supports the suggestion that the nonmigrating tide DE3 is the origin of the corresponding longitudinal structure in the ionosphere.

[19] **Acknowledgments.** The ROCSAT-1 data is provided by S.-Y. Su at the National Central University, Chung-Li, Taiwan. We are grateful to the SABER team for the access to the data on http://saber.gats-inc.com; we are also grateful to the TIDI team for the access to the data on http://timed.hao.ucar.edu/tidi. This work is supported by the KIP Pilot Project (kzcx2-yw-123) of CAS, National Important Basic Research Project (2006CB806306), and National Science Foundation of China (40636032, 40725014).

[20] Zuyin Pu thanks Scott England and another reviewer for their assistance in evaluating this manuscript.

References

England, S. L., T. J. Immel, E. Sagawa, S. B. Henderson, M. E. Hagan, S. B. Mende, H. U. Frey, C. M. Swenson, and L. J. Paxton (2006a), Effect of atmospheric tides on the morphology of the quiet time, postsunset equatorial ionospheric anomaly, *J. Geophys. Res.*, *111*, A10S19, doi:10.1029/2006JA011795.

England, S. L., S. Maus, T. J. Immel, and S. B. Mende (2006b), Longitudinal variation of the *E* region electric fields caused by atmospheric tides, *Geophys. Res. Lett.*, *33*, L21105, doi:10.1029/2006GL027465.

England, S. L., T. J. Immel, and J. D. Huba (2008), Modeling the longitudinal variation in the post-sunset far-ultraviolet OI airglow using the SAMI2 model, *J. Geophys. Res.*, *113*, A01309, doi:10.1029/2007JA012536.

Fejer, B. G., J. W. Jensen, and S.-Y. Su (2008), Quiet time equatorial *F* region vertical plasma drift model derived from ROCSAT-1 observations, *J. Geophys. Res.*, *113*, A05304, doi:10.1029/2007JA012801.

Forbes, J. M., M. E. Hagan, S. Miyahara, Y. Miyoshi, and X. Zhang (2003a), Diurnal nonmigrating tides in the tropical lower thermosphere, *Earth Planets Space*, *55*, 419–426.

Forbes, J. M., X. Zhang, E. R. Talaat, and W. Ward (2003b), Nonmigrating diurnal tides in the thermosphere, *J. Geophys. Res.*, *108*(A1), 1033, doi:10.1029/2002JA009262.

Forbes, J. M., X. Zhang, S. Palo, J. Russell, C. J. Mertens, and M. Mlynczak (2008), Tidal variability in the ionospheric dynamo region, *J. Geophys. Res.*, *113*, A02310, doi:10.1029/2007JA012737.

Hagan, M. E., and J. M. Forbes (2002), Migrating and nonmigrating diurnal tides in the middle and upper atmosphere excited by tropospheric latent heat release, *J. Geophys. Res.*, *107*(D24), 4754, doi:10.1029/2001JD001236.

Hagan, M. E., and J. M. Forbes (2003), Migrating and nonmigrating semidiurnal tides in the upper atmosphere excited by tropospheric latent heat release, *J. Geophys. Res.*, *108*(A2), 1062, doi:10.1029/2002JA009466.

Hagan, M. E., A. Maute, R. G. Roble, A. D. Richmond, T. J. Immel, and S. L. England (2007), Connections between deep tropical clouds and the Earth's ionosphere, *Geophys. Res. Lett.*, *34*, L20109, doi:10.1029/2007GL030142.

Hartman, W. A., and R. A. Heelis (2007), Longitudinal variations in the equatorial vertical drift in the topside ionosphere, *J. Geophys. Res.*, *112*, A03305, doi:10.1029/2006JA011773.

Heelis, R. A. (2004), Electrodynamics in the low and middle latitude ionosphere: A tutorial, *J. Atmos. Sol. Terr. Phys.*, *66*(10), 825–838, doi:10.1016/j.jastp.2004.01.034.

Henderson, S. B., C. M. Swenson, A. B. Christensen, and L. J. Paxton (2005), Morphology of the equatorial anomaly and equatorial plasma bubbles using image subspace analysis of Global Ultraviolet Imager data, *J. Geophys. Res.*, *110*, A11306, doi:10.1029/2005JA011080.

Immel, T. J., E. Sagawa, S. L. England, S. B. Henderson, M. E. Hagan, S. B. Mende, H. U. Frey, C. M. Swenson, and L. J. Paxton (2006), Control of equatorial ionospheric morphology by atmospheric tides, *Geophys. Res. Lett.*, *33*, L15108, doi:10.1029/2006GL026161.

Jin, H., Y. Miyoshi, H. Fujiwara, and H. Shinagawa (2008), Electrodynamics of the formation of ionospheric wave number 4 longitudinal structure, *J. Geophys. Res.*, *113*, A09307, doi:10.1029/2008JA013301.

Kil, H., S.-J. Oh, M. C. Kelley, L. J. Paxton, S. L. England, E. Talaat, K.-W. Min, and S.-Y. Su (2007), Longitudinal structure of the vertical $\mathbf{E} \times \mathbf{B}$ drift and ion density seen from ROCSAT-1, *Geophys. Res. Lett.*, *34*, L14110, doi:10.1029/2007GL030018.

Kil, H., E. R. Talaat, S.-J. Oh, L. J. Paxton, S. L. England, and S.-J. Su (2008), Wave structures of the plasma density and vertical $\mathbf{E} \times \mathbf{B}$ drift in low-latitude *F* region, *J. Geophys. Res.*, *113*, A09312, doi:10.1029/2008JA013106.

Killeen, T. L., et al. (1999), TIMED Doppler Interferometer (TIDI), *Proc. SPIE*, *3756*, 289–301, doi:10.1117/12.366383.

Li, G., B. Ning, L. Liu, B. Zhao, X. Yue, S.-Y. Su, and S. Venkatraman (2008), Correlative study of plasma bubbles, evening equatorial ionization anomaly, and equatorial prereversal $\mathbf{E} \times \mathbf{B}$ drifts at solar maximum, *Radio Sci.*, *43*, RS4005, doi:10.1029/2007RS003760.

Lin, C. H., W. Wang, M. E. Hagan, C. C. Hsiao, T. J. Immel, M. L. Hsu, J. Y. Liu, L. J. Paxton, T. W. Fang, and C. H. Liu (2007a), Plausible effect of atmospheric tides on the equatorial ionosphere observed by the FORMOSAT-3/COSMIC: Three-dimensional electron density structures, *Geophys. Res. Lett.*, *34*, L11112, doi:10.1029/2007GL029265.

Lin, C. H., C. C. Hsiao, J. Y. Liu, and C. H. Liu (2007b), Longitudinal structure of the equatorial ionosphere: Time evolution of the four-peaked EIA structure, *J. Geophys. Res.*, *112*, A12305, doi:10.1029/2007JA012455.

Liu, H., and S. Watanabe (2008), Seasonal variation of the longitudinal structure of the equatorial ionosphere: Does it reflect tidal influences from below?, *J. Geophys. Res.*, *113*, A08315, doi:10.1029/2008JA013027.

Liu, L., M. He, W. Wan, and M.-L. Zhang (2008), Topside ionospheric scale heights retrieved from Constellation Observing System for Meteorology, Ionosphere, and Climate radio occultation measurements, *J. Geophys. Res.*, *113*, A10304, doi:10.1029/2008JA013490.

Liu, L., B. Zhao, W. Wan, B. Ning, M.-L. Zhang, and M. He (2009), Seasonal variations of the ionospheric electron densities retrieved from Constellation Observing System for Meteorology, Ionosphere, and Climate mission radio occultation measurements, *J. Geophys. Res.*, *114*, A02302, doi:10.1029/2008JA013819.

Lühr, H., K. Häusler, and C. Stolle (2007), Longitudinal variation of *F* region electron density and thermospheric zonal wind caused by atmospheric tides, *Geophys. Res. Lett.*, *34*, L16102, doi:10.1029/2007GL030639.

Lühr, H., M. Rother, K. Hausler, P. Alken, and S. Mausi (2008), Influence of nonmigrating tides on the longitudinal variation of the equatorial electrojet, *J. Geophys. Res.*, *113*, A08313, doi:10.1029/2008JA013064.

Oberheide, J., and J. M. Forbes (2008a), Tidal propagation of deep tropical cloud signatures into the thermosphere, *Geophys. Res. Lett.*, *35*, L04816, doi:10.1029/2007GL032397.

Oberheide, J., and J. M. Forbes (2008b), Thermospheric nitric oxide variability induced by nonmigrating tides, *Geophys. Res. Lett.*, *35*, L16814, doi:10.1029/2008GL034825.

Oberheide, J., Q. Wu, T. L. Killeen, M. E. Hagan, and R. G. Roble (2006), Diurnal nonmigrating tides from TIMED Doppler Interferometer wind data: Monthly climatologies and seasonal variations, *J. Geophys. Res.*, *111*, A10S03, doi:10.1029/2005JA011491.

Oh, S.-J., H. Kil, W.-T. Kim, L. J. Paxton, and Y. H. Kim (2008), The role of the vertical $\mathbf{E} \times \mathbf{B}$ drift for the formation of the longitudinal plasma density structure in the low-latitude *F* region, *Ann. Geophys.*, *26*, 2061–2067.

Pedatella, N. M., J. M. Forbes, and J. Oberheide (2008), Intra-annual variability of the low-latitude ionosphere due to nonmigrating tides, *Geophys. Res. Lett.*, *35*, L18104, doi:10.1029/2008GL035332.

Ren, Z., W. Wan, L. Liu, B. Zhao, Y. Wei, X. Yue, and R. A. Heelis (2008), Longitudinal variations of electron temperature and total ion density in the sunset equatorial topside ionosphere, *Geophys. Res. Lett.*, *35*, L05108, doi:10.1029/2007GL032998.

Richmond, A. D., and R. G. Roble (1987), Electrodynamic effects of thermospheric winds from the NCAR thermospheric general circulation model, *J. Geophys. Res.*, *92*(A11), 12,365–12,376, doi:10.1029/JA092iA11p12365.

Russell, M., III, M. Mlynczak, M. G. Gordley, L. L. Tansock, and J. Esplin (1999), An overview of the SABER experiment and preliminary calibration results, *Proc. SPIE Int. Soc. Opt. Eng.*, *3756*, 277–288.

Sagawa, E., T. J. Immel, H. U. Frey, and S. B. Mende (2005), Longitudinal structure of the equatorial anomaly in the nighttime ionosphere observed by IMAGE/FUV, *J. Geophys. Res.*, *110*, A11302, doi:10.1029/2004JA010848.

Scherliess, L., D. C. Thompson, and R. W. Schunk (2008), Longitudinal variability of low-latitude total electron content: Tidal influences, *J. Geophys. Res.*, *113*, A01311, doi:10.1029/2007JA012480.

Wan, W., L. Liu, X. Pi, M.-L. Zhang, B. Ning, J. Xiong, and F. Ding (2008), Wavenumber 4 patterns of the total electron content over the low latitude ionosphere, *Geophys. Res. Lett.*, *35*, L12104, doi:10.1029/2008GL033755.

L. Liu, Z. Ren, W. Wan, and J. Xiong, Beijing National Observatory of Space Environment, Institute of Geology and Geophysics, Chinese Academy of Sciences, Beijing, 100029, China. (wanw@mail.iggcas.ac.cn)